Journal of Power Sources 191 (2009) 225–232

Contents lists available at ScienceDirect

Journal of Power Sources

journal homepage: www.elsevier.com/locate/jpowsour

A comparative study of $La_{0.8}Sr_{0.2}MnO_3$ and $La_{0.8}Sr_{0.2}Sc_{0.1}Mn_{0.9}O_3$ as cathode materials of single-chamber SOFCs operating on a methane–air mixture

Chunming Zhang [a], Yao Zheng [a], Ye Lin [a], Ran Ran [a], Zongping Shao [a,*], David Farrusseng [b]

[a] State Key Laboratory of Materials-Oriented Chemical Engineering, Nanjing University of Technology No.5 Xin Mofan Road, Nanjing, JiangSu 210009, PR China
[b] IRCELYON, Institut de recherches sur la catalyse et l'environnement de Lyon, Unit'e Mixte de Recherche 5256 CNRS-Universit'e de Lyon 1, 2 avenue Albert Einstein, F-69626 Villeurbanne Cedex, France

ARTICLE INFO

Article history:
Received 10 January 2009
Received in revised form 16 February 2009
Accepted 16 February 2009
Available online 3 March 2009

Keywords:
Single chamber
Solid oxide fuel cells
Cathode
Methane
Initialization

ABSTRACT

As candidates of cathode materials for single-chamber solid oxide fuel cells, $La_{0.8}Sr_{0.2}MnO_3$ (LSM) and $La_{0.8}Sr_{0.2}Sc_{0.1}Mn_{0.9}O_3$ (LSSM) were synthesized by a combined EDTA-citrate complexing sol–gel process. The solid precursors of LSM and LSSM were calcined at 1000 and 1150 °C, respectively, to obtain products with similar specific surface area. LSSM was found to have higher activity for methane oxidization than LSM due to LSSM's higher catalytic activity for oxygen reduction. Single cells with these two cathodes initialized by ex situ reduction had similar peak power densities of around 220 mW cm^{-2} at 825 °C. The cell using the LSM cathode showed higher open-circuit-voltage (OCV) at corresponding temperatures due to its reduced activity for methane oxidation relative to LSSM. A negligible effect of methane and CO_2 on the cathode performance was observed for both LSM and LSSM via electrochemical impedance spectroscopy analysis. The high phase stability of LSSM under reducing atmosphere allows a more convenient in situ reduction for fuel cell initiation. The resultant cell with LSSM cathode delivered a peak power density of ~200 mW cm^{-2} at 825 °C, comparable to that from ex situ reduction.

© 2009 Elsevier B.V. All rights reserved.

1. Introduction

In recent years, single-chamber solid oxide fuel cells (SC-SOFCs) have been receiving attention for their simplified reactor configuration and capability for quick start-up. They have potential application as micropower generator for portable devices. Because they operate on fuel–air mixture, one way to minimize the gas phase reaction that would reduce the electrical efficiency is to adopt fuels with high chemical stability such as hydrocarbons with low carbon numbers, especially methane [1–7]; another way is to reduce the operation temperature.

The operation principle of methane-fueled SC-SOFCs relies on different chemical catalytic and electro-catalytic activities of anode and cathode materials in the methane–air mixture [8–10]. Ideally, the cathode is inert to the oxidation of methane but highly efficient for oxygen reduction (Eq. (1)), while the anode possesses high catalytic activity and selectivity towards partial oxidation of methane, forming CO and H_2 (Eq. (2)). During operation, the oxygen anion is pumped from the cathode side through electrolyte and reacted with CO and H_2 at the anode to produce electricity (Eqs. (3) and (4)).

$$0.5O_2 + 2e^- \rightarrow O^{2-} \quad (1)$$

$$2CH_4 + O_2 \rightarrow 2CO + 4H_2 \quad (2)$$

$$CO + O^{2-} \rightarrow CO_2 + 2e^- \quad (3)$$

$$H_2 + O^{2-} \rightarrow H_2O + 2e^- \quad (4)$$

Because of their large number of bulk oxygen vacancies, cobalt-based perovskite oxides like $La_{0.6}Sr_{0.4}CoO_{3-\delta}$ (LSC), $La_{0.6}Sr_{0.4}Co_{0.8}Fe_{0.2}O_{3-\delta}$ (LSCF), $Sm_{0.5}Sr_{0.5}CoO_{3-\delta}$ (SSC) and $Ba_{0.5}Sr_{0.5}Co_{0.8}Fe_{0.2}O_{3-\delta}$ (BSCF), have been extensively investigated as cathode materials in dual-chamber SOFCs (DC-SOFCs) [11–15]. Good performance at intermediate temperature has been achieved in many reports. However, such materials are intrinsically unstable in reducing atmosphere. For example, BSCF can be reduced to metallic Co, Fe and $BaO/Ba(OH)_2{\cdot}xH_2O$, $SrO/(Sr(OH)_2{\cdot}xH_2O$ under hydrogen atmosphere [16]. If these materials are applied as the cathode of SC-SOFCs, an additional ex situ reduction step is preferred to avoid destruction of the perovskite lattice structure by the reducing atmosphere during the initialization process [17–19]. The so-called ex situ reduction is a pre-reducing process for the anode substrate, mostly from NiO to Ni, before the deposition of cathode on the electrolyte layer. When applying the ex situ reduction process, to avoid the re-oxidation of the Ni-based anode, after the cathode deposition is completed, the three layered cell must be fired under an inert atmosphere to adhere the cathode onto the electrolyte surface firmly. However, such a SC-SOFC fabrication process is time consuming and expensive.

* Corresponding author. Tel.: +86 25 83172256; fax: +86 25 83172256.
E-mail address: shaozp@njut.edu.cn (Z. Shao).

0378-7753/$ – see front matter © 2009 Elsevier B.V. All rights reserved.
doi:10.1016/j.jpowsour.2009.02.043

In our previous work, a simplified in situ reduction process was introduced to initialize SC-SOFCs, in which both the unreduced anode and cathode were exposed to the same reducing atmosphere of hydrogen [20]. If successful, the conventional fuel cell fabrication technique could also be applied for the SC-SOFCs, thereby greatly reducing the fabrication cost. However, the initiation by in situ reduction did not work well for SC-SOFCs with a BSCF cathode. Although a reduced BSCF cathode can be partially restored to its initial perovskite structure under a methane–air atmosphere at high temperatures, the power output of the cells was much lower than that of the cell initialized by ex situ reduction due to the altered electrode structure after the reduction/re-oxidation process. Thus, there is an urgent need for the development of a more stable cathode for the reducing atmosphere.

As a classic cathode material of DC-SOFCs, $La_{0.8}Sr_{0.2}MnO_3$ (LSM) shows good structural and chemical stability under cathodic operation condition. It has been applied as the cathode of SC-SOFC by Hibino et al., who reported a peak power density of 204 mW cm^{-2} at a furnace temperature of 950 °C for a cell with 15 wt.% MnO_2-modified $La_{0.8}Sr_{0.2}MnO_3$ as cathode when operating in a methane–air mixture [8]. The decomposition oxygen partial pressure of LSM is around 10^{-18} atm at 800 °C [21], suggesting that the stability of LSM may still be a problem in SC-SOFC applications when adopting the in situ reduction process for cell initialization, since the oxygen partial pressure in a hydrogen atmosphere could be lower than 10^{-19} atm. Recently, we have developed a novel perovskite-type oxide $La_{0.8}Sr_{0.2}Sc_{0.1}Mn_{0.9}O_3$ (LSSM) which showed not only better cathode performance than LSM for electrochemical oxygen reduction [22–25] but also improved stability under reducing atmosphere [24]. Yue et al. also reported this cathode material which had better performance [26]. This suggests that LSSM may be a potential candidate for an SC-SOFC cathode.

In this paper, LSM and LSSM were prepared and their performance in SC-SOFCs operating in a methane–air mixture was systematically investigated. The cell initialization by both ex situ and in situ reduction methods for the two cells was comparatively studied.

2. Experimental

2.1. Powder synthesis and fuel cell fabrication

The fuel cells employed in this study were in an anode-supported configuration with a NiO + ScSZ anode substrate (~500 μm, NiO:ScSZ = 60:40 by wt.%), ScSZ electrolyte (20–30 μm) and an LSM or LSSM cathode (~20 μm). ScSZ, LSM and LSSM were all synthesized by a combined EDTA-citrate complexing sol–gel process. Such a preparation process has been described in detail in our previous publications [27,28]. A dry-pressing/sintering process was adopted to fabricate the anode-supported thin-film ScSZ bi-layer pellets. These green dual-layer pellets resulting from dry pressing were then fired at 1500 °C for 5 h in air to achieve the densification of the electrolyte layer and a firm connection between the anode substrate and the thin-film electrolyte. The cathode was applied to the electrolyte surface by a spray deposition/sintering process. The cathode powder (LSM or LSSM) was first dispersed in a pre-mixed solution of glycerol, ethylene glycol and isopropyl alcohol to form a colloidal suspension through high-energy ball milling (Fritsch, Pulverisette 6), at a rotational speed of 400 rpm for 1 h. The resultant slurry was spray deposited onto the electrolyte surface of fresh or pre-reduced dual-layer membranes, then calcined at 1000 °C (the resulting sample was named LSM_{1000}) and 1150 °C ($LSSM_{1150}$) for 2 h in air (or under a flowing nitrogen atmosphere for the cells with a pre-reduced anode) to obtain triple-layered single cells. The resulting coin-shaped cathode had an effective geometric surface area of 0.48 cm^2.

2.2. Catalytic characterization

The catalytic activity of the LSM or LSSM for methane oxidation was evaluated in a flow-through fixed bed reactor, which is composed of a quartz tube with an inner diameter of ~8 mm. About 0.02 g of catalyst (60–80 mesh LSM or LSSM particulates) was put in the center of the reactor. A K-type thermocouple with the protection of a small quartz tube was immersed into the catalyst bed to monitor the reaction temperature. A tube furnace was applied to sustain the temperature required for the reaction. Methane–oxygen–helium mixed gas in a ratio of 1.3:1:4 was introduced from the top of the reactor. The effluent gas from the bottom of the reactor was introduced to a Varian 3800 gas chromatograph, which was equipped with Poraplot Q and 5 Å molecular sieve capillary columns for the separation of H_2, O_2, CO, CO_2 and CH_4. Before introduction into the reactor, water was adsorbed by a cooling trap. The methane and oxygen conversions were calculated based on:

$$\%\text{conversion}_{CH_4} = \frac{[CO] + [CO_2]}{[CO] + [CO_2] + [CH_4]_{outlet}} \times 100$$

$$\%\text{conversion}_{O_2} = \frac{0.5[CO] + [CO_2] + 0.5[H_2O]}{0.5[CO] + [CO_2] + 0.5[H_2O] + [O_2]_{outlet}} \times 100$$

2.3. Fuel cell performance test

Fuel cell polarization curves were obtained at furnace temperatures of 750–850 °C. The gas was composed of methane, oxygen and nitrogen at flow rates of 110, 85 and 340 ml min^{-1} [STP], respectively. *I–V* polarization curves were collected using a Keithley 2420 source meter based on the four-terminal configuration.

Electrochemical characterization of LSM and LSSM as cathode materials on a ScSZ electrolyte was conducted based on a three-electrode configuration using an electrochemical workstation composed of a Solartron 1287 Potentiostat and a Solartron 1260A Frequency Response Analyzer. The frequency applied ranged from 0.1 Hz to 100 kHz, and the signal amplitude was 10 mV. The thickness and diameter of the sintered electrolyte disks were ~0.3 and 16 mm, respectively. Isopropyl alcohol-based LSM or LSSM slurry was applied to one side of electrolyte substrate by spray deposition and then calcined at 1000 or 1150 °C in air for 2 h to act as the working electrode. An Ag paste was adopted as the current collector of the working electrode. Silver paste was also used as the reference electrode by painting a ring around the Pt counter electrode on the other side of the electrolyte pellet. The gap between the counter and reference electrodes was ~4 mm. The areas of the working, counter and reference electrodes were 0.26, 0.26 and 0.3 cm^2, respectively. The cathodic resistances were tested under a constant cathodic current of 400 mA cm^{-2}.

2.4. Other characterization

The BET (Brunauer–Emmett–Teller) surface area of the samples was characterized by N_2 adsorption at the temperature of liquid nitrogen using a BELSORP II instrument. Prior to analysis, the samples were put in vacuum at 200 °C for 3–5 h to remove the surface adsorbed species. An X-ray diffractometer (XRD, Bruker D8 Advance) was used to analyze the stability of LSM and LSSM against a reducing atmosphere during the process of in situ reduction. The diffractometer operated at 40 kV and 30 mA using Cu Kα radiation with a wavelength of 1.5418 Å, with a scanning angle (Bragg angle 2θ) ranging from 20° to 80° at a rate of 0.05° s^{-1}. The microscopic features of the electrodes were characterized using an environmental scanning electron microscope (ESEM, JSM-5610LV).

3. Results and discussion

3.1. Special surface areas and catalytic activities

The grain size and morphology of the catalysts typically have a significant effect on their catalytic activity [29]. A high specific surface area means more active sites, and thus a higher catalytic activity. In this study, the increase of sintering temperature led to a decreasing specific surface area. Furthermore, a much larger specific surface area of LSSM than LSM at the same calcination temperature was observed, which is likely associated with the excessive amount of HNO_3 added for dissolving Sc_2O_3 in the synthesis of LSSM powder. The excessive HNO_3 can react with $NH_3{\cdot}H_2O$ to form NH_4NO_3, which is a fine combustion aid in the later pre-fired process [30]. The huge amount of gases produced during combustion can separate the product particles and then effectively suppress their segregation. To obtain a reasonable comparison of the catalytic activity, the sintering temperatures of 1000 °C for LSM (BET surface area of ~1.23 $m^2\ g^{-1}$) and 1150 °C for LSSM (BET surface area is ~1.50 $m^2\ g^{-1}$) were chosen to obtain powders with similar specific surface area. These two temperatures were also selected for the fabrication of LSM and LSSM onto the electrolyte surfaces for cell performance tests.

Based on Nernst equation, the open-circuit-voltage (OCV) is closely related to the oxygen partial pressure (P_{O_2}) around the electrode surfaces. An ideal cathode material for SC-SOFC should possess high electro-catalytic activity for oxygen reduction but low activity for fuel oxidation. The catalytic activities of the LSM and LSSM powders with similar specific surface areas were then evaluated as a function of operating temperature (600–900 °C). The molar ratio of methane to oxygen was 1.3:1 (He 40 ml min^{-1}, CH_4 13 ml min^{-1}, O_2 10 ml min^{-1}) to simulate the gas composition in a SC-SOFC [20]. Here, helium was applied to replace nitrogen for GC analysis purposes.

Fig. 1 shows that the conversions of methane and oxygen over an LSSM catalyst are much larger than those of an LSM at the same temperature. This indicates that LSSM had higher catalytic activity than LSM for methane oxidization. Since these two samples had similar morphologies and surface areas, their different activities could be attributed to intrinsic properties such as oxygen reduction capability. It is widely known that the catalytic activity of oxides is closely related to the oxygen reduction capability and especially, the surface concentration of oxygen vacancies [31]. The oxygen vacancies can influence the capacity of oxygen adsorption sites and species on the catalyst (or electrode) surface. The two different models describing this complex reaction process are the Mars van Krevlen

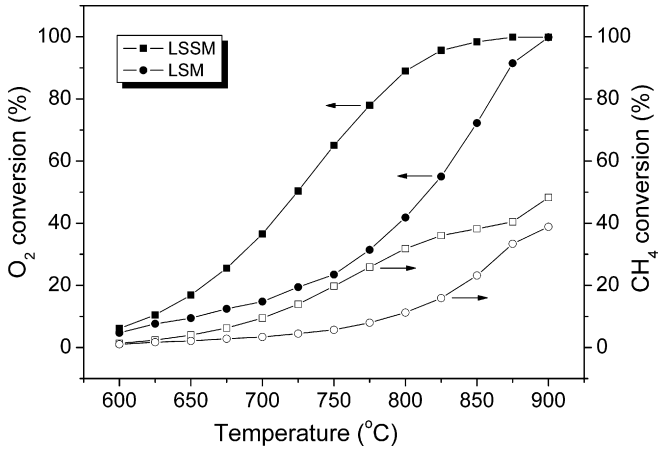

Fig. 1. The conversions of methane and oxygen at various temperatures for both LSM and LSSM catalysts (He 40 ml min^{-1}, CH_4 13 ml min^{-1}, O_2 10 ml min^{-1}).

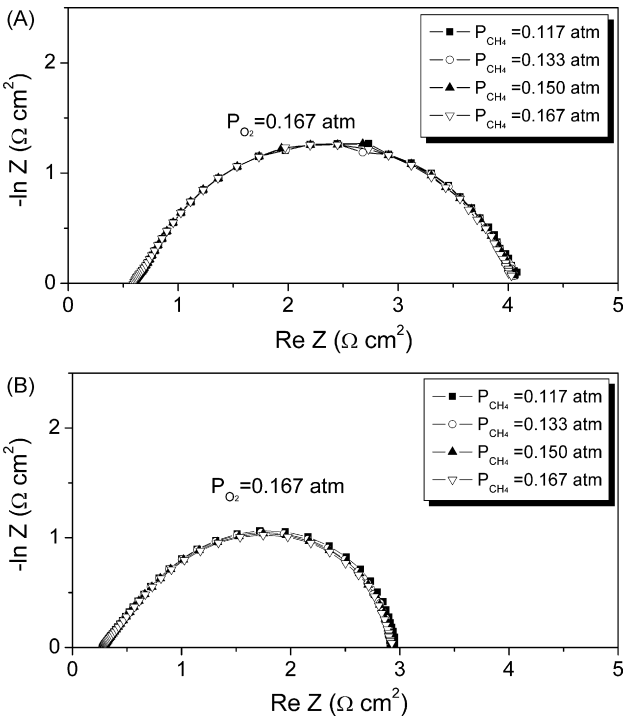

Fig. 2. The EIS of LSM (A) and LSSM (B) under a CH_4–O_2 mixture with different methane partial pressure and a fixed oxygen partial pressure of 0.167 atm at 800 °C before polarization.

(MvK) and Ionic Redox (IoR) models [32,33]. In brief, the MvK model takes into consideration that the reactant is adsorbed and oxidized at some active sites and that the reduced catalyst is then re-oxidized by gas phase molecular oxygen at the same sites. Adsorption of molecular oxygen is assumed to be the rate-limiting step of the overall reaction. The other model believes that the reduction and re-oxidation occur on different sites of the catalyst surface, and that the re-oxidation reactant is not gas oxygen, but lattice oxygen transferred through the oxygen vacancy to the active site of the catalyst surface.

The catalytic activity of an oxide is closely related to the concentration of oxygen vacancy on its surface. In general, the more oxygen vacancies, the higher catalytic activity in oxygen reduction will be for the oxide. If the vacancies are occupied by other insulating things including gases such as carbon dioxide and methane, the sites for oxygen reduction will be partially blocked with consequently dropping in electro-catalytic activity in oxygen reduction reaction (ORR). The electrochemical impedance spectroscopy (EIS) is an effective technique to characterize the ORR on a cathode, so it is expected that the catalytic activity of the oxide can be indirectly characterized by the EIS. To demonstrate whether oxygen and methane are adsorbed over the same active sites, the EIS of LSM and LSSM oxides under methane–oxygen mixed gases was measured. The oxygen partial pressure of the atmosphere was kept at 0.167 atm while the methane partial pressure was varied. To minimize the influence of methane oxidation over the cathode, which could have an impact on the EIS, the methane and oxygen flow rate was kept high to keep the methane conversion under 10%. As shown in Fig. 2, the methane had almost no impact on the electrochemical oxygen reduction over both cathodes at 800 °C. This likely suggests that methane and oxygen had different adsorption sites. Therefore, the IoR model more precisely describes the methane oxidation over LSM and LSSM cathodes.

Based on the IoR model, the oxygen surface exchange kinetic and bulk oxygen ion conductivity are crucial parameters for the oxide

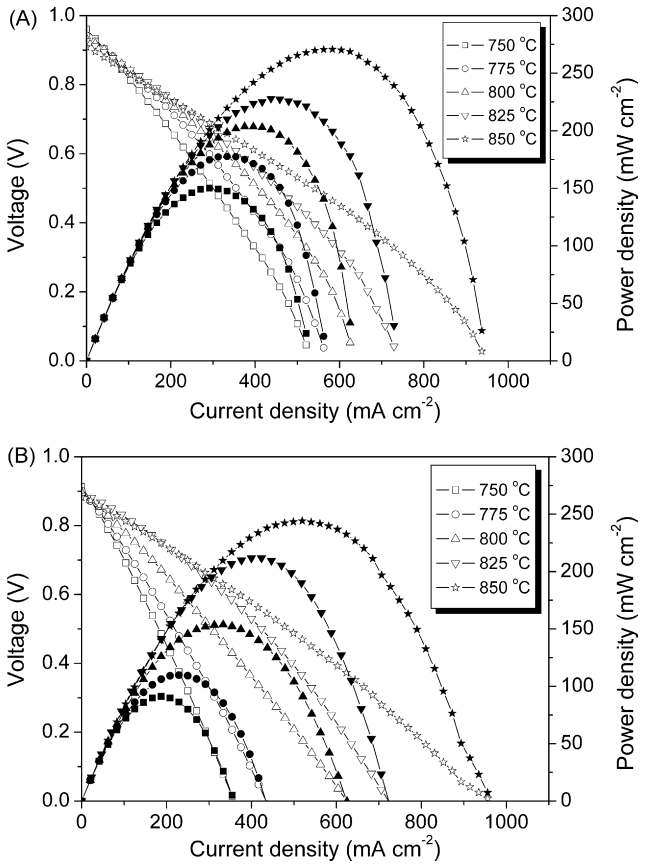

Fig. 3. The *I–V* and *I–P* curves of the cells with LSM (A) and LSSM (B) cathodes tested at 750–850 °C using the ex situ initialized method.

catalyst. The higher the surface activity for oxygen reduction and the higher the oxygen bulk diffusion rate, the higher the methane oxidation rate should be. Since LSSM has a higher bulk and surface oxygen vacancy concentration than LSM [25], it follows that LSSM should have more catalytic activity than LSM for methane oxidation. Their different catalytic activities towards methane oxidation may cause differences in the oxygen partial pressure over the cathode surface, as well as the different OCVs of the SC-SOFCs. Such influence will be discussed in detail later.

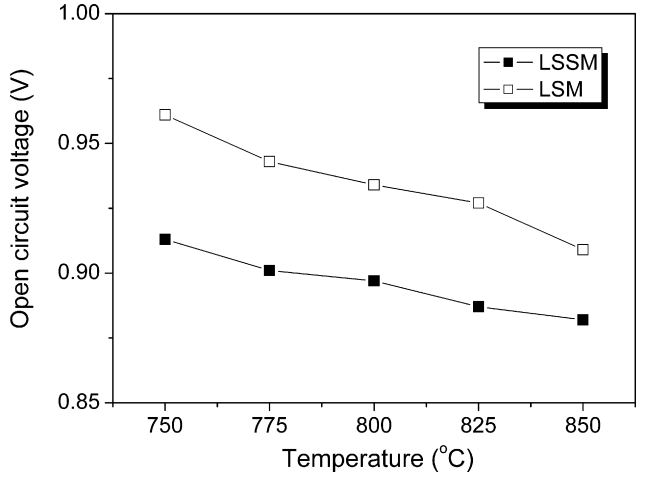

Fig. 4. The OCVs of the two cells with LSM and LSSM cathode at operation temperatures.

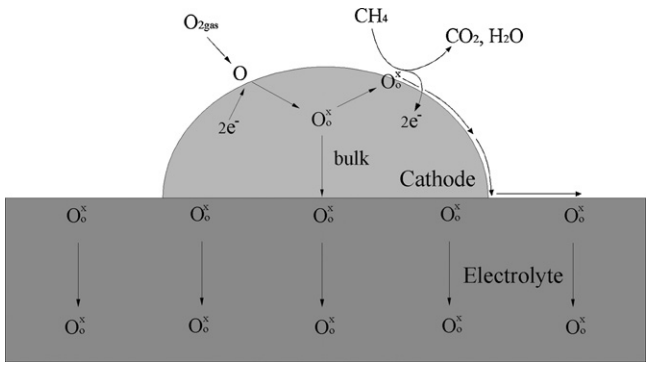

Fig. 5. The reaction mechanism of methane and oxygen mixed gases on the surface of perovskite catalysts.

3.2. Electrochemical performance of the cells based on ex situ reduction

The current–voltage (*I–V*) and current–power (*I–P*) curves of the cells with these two cathodes initialized by the ex situ reduction method were first comparatively tested at 750–850 °C (furnace temperature) with the results shown in Fig. 3. For the cell with the LSM cathode (cell A), the peak power densities (PPDs) reached 275 and 225 mW cm^{-2} at 850 and 825 °C, respectively, which are slightly higher values than those of the cell with the LSSM cathode (cell B). As shown in Fig. 4, the OCVs of these two cells decreased monotonously with increasing temperature, indicating the methane was actually oxidized via an indirect oxidization mechanism, i.e., it was first partially oxidized to CO and H_2, which were then oxidized to H_2O and CO_2 over the anode to produce electricity (Eqs. (2)–(4)). Within the temperature range tested, the OCVs of cell A were about 0.03–0.05 V higher than those of cell B are.

During the fuel cell operation, molecular oxygen was first adsorbed over the cathode surface and then dissociated into two

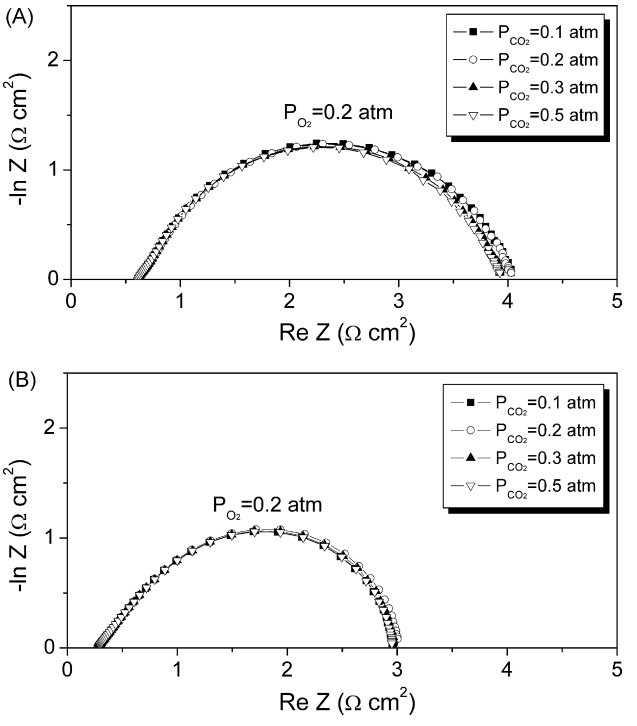

Fig. 6. The EIS of LSM (A) and LSSM (B) at 800 °C before polarization under various atmospheres composed of CO_2 and O_2 with varied CO_2 concentration but fixed oxygen partial pressure of 0.2 atm.

oxygen atoms, which combined with electrons to generate lattice oxygen ($O_O^{\times}$). In DC-SOFCs, the $O_O^{\times}$ diffuse through to the bulk of cathode or diffuse around the electrode surface to the electrolyte surface, and are then transported further through the electrolyte and reacted with fuel over the anode surface to produce electricity (step 1, as shown in Fig. 5). However, in the SC-SOFC operation model, the created oxygen ion was also able to proceed in an additional pathway, i.e., the $O_O^{\times}$ diffused back to the oxide surface and reacted with methane to form carbon dioxide and water (step 2). These two reactions preceeded in parallel. The excessive consumption of $O_O^{\times}$ by step 2 resulted in a decreasing concentration of adsorbed oxygen over the perovskite surface. Based on the Nernst equation, the OCV depends on the difference of oxygen partial pressure between the anode and the cathode. Since the LSSM had a higher catalytic activity for methane oxidation, it consumed more adsorbed oxygen than the LSM. Thereby, a lower surface oxygen potential over LSSM than LSM cathode was expected, which then led to a lower OCV.

3.3. Adsorption behavior of carbon dioxide

It is well known that carbon dioxide could have a strong effect on the cathodic performance of some perovskite oxides such as BSCF, at intermediate temperature. Since the methane oxidation would produce CO_2, the effect of CO_2 on the cathode performance over LSM and LSSM needs to be clarified. Fig. 6 shows the EIS of LSM and LSSM at 800 °C before polarization under various atmospheres composed of CO_2 and O_2 with varied CO_2 concentration but fixed oxygen partial pressure at 0.2 atm. It demonstrates that the sizes of EIS changed little with varying carbon dioxide partial pressure (P_{CO_2}), especially for the LSSM cathode. This is significantly different from that of the BSCF cathode [34,35]. Such a feature is beneficial for single-chamber application since CO_2 is avoidable in single-chamber fuel cell reactor. Some reports in the literature indicate that there was SrO segregation over perovskite oxide surfaces

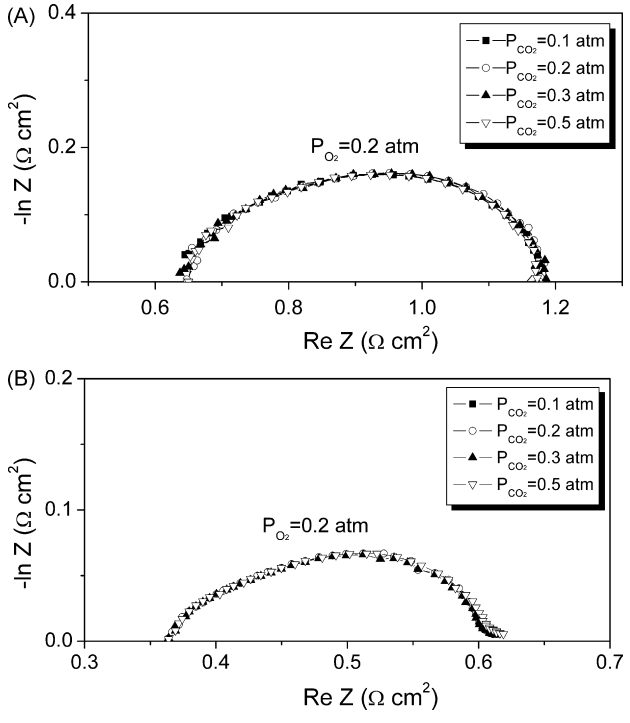

Fig. 7. The EIS of LSM (A) and LSSM (B) at 800 °C under various atmospheres composed of CO_2 and O_2 with varied CO_2 concentration but fixed oxygen partial pressure of 0.2 atm after the polarization under a constant current of −400 mA cm^{-2}.

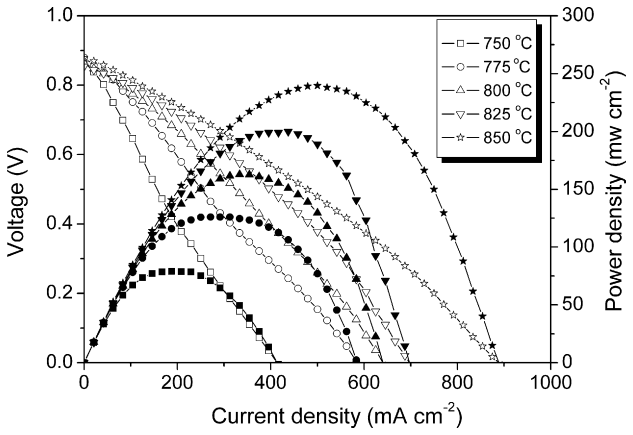

Fig. 8. The *I–V* and *I–P* curves of the cell with LSSM cathode testing at 750–850 °C using the in situ initialized method.

such as LSM [21,36] and LSCF [37]. The small variation in polarization resistance with varying P_{CO_2} for an LSM cathode is then likely associated with the adsorption of carbon dioxide on such surface enriched with SrO.

Fig. 7 shows the effect of CO_2 on the oxygen reduction activity of LSM and LSSM cathodes after polarization. After polarization at a cathodic current of 400 mA cm^{-2}, the electrode polarization resistance reduced significantly due to the increasing amount of in situ created oxygen vacancies in the bulk and over the surface of the electrode [38,39]. Furthermore, the sensitivity of the EIS with respect to carbon dioxide decreased slightly after polarization, which was attributed to the fact that the surface enriched SrO was incorporated into the LSM lattice during the cathodic polarization [40]. Comparing the results in Figs. 6B and 7B, the degree of resistance variation with varying P_{CO_2} for the LSSM cathode was smaller than that for the LSM. This may be explained by the fact that the SrO generation over perovskite oxides surface was suppressed by the Sc^{3+} doping [22]. By this token, one significant advantage of LSM-based electrodes, especially LSSM, over BSCF is their better capacity to resist carbon dioxide poisoning.

3.4. Fuel cell performance adopting in situ reduction

Another advantage of LSM-based electrodes over Co-based electrodes such as SSC and BSCF in single-chamber operation may be their better chemical stability against a reducing atmosphere. This suggests that the fuel cells with LSM-based electrodes may adopt a convenient in situ reduction initialization. Fig. 8 shows the *I–V* and

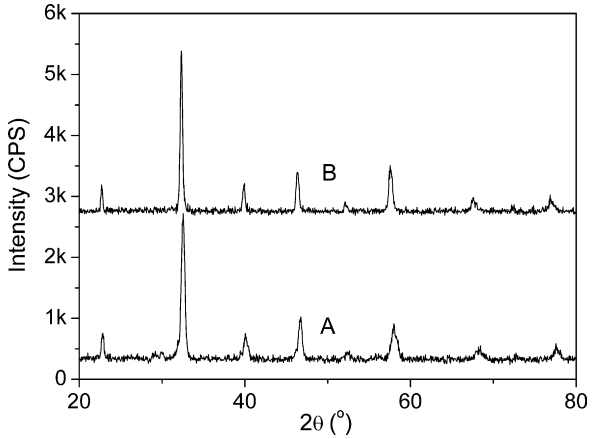

Fig. 9. XRD patterns of LSSM material before and after pre-treatment with hydrogen gas (A) LSSM fresh and (B) LSSM reduced by hydrogen at 600 °C for 1 h.

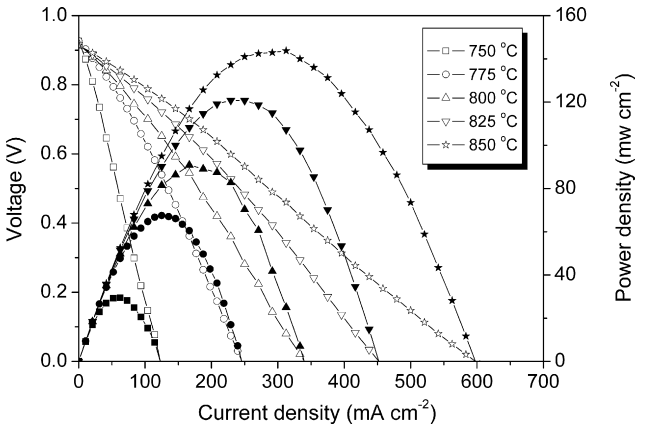

Fig. 10. The *I–V* and *I–P* curves of the cell with an LSM cathode that had been pre-treated in hydrogen gas and then exposed at the testing atmospheres.

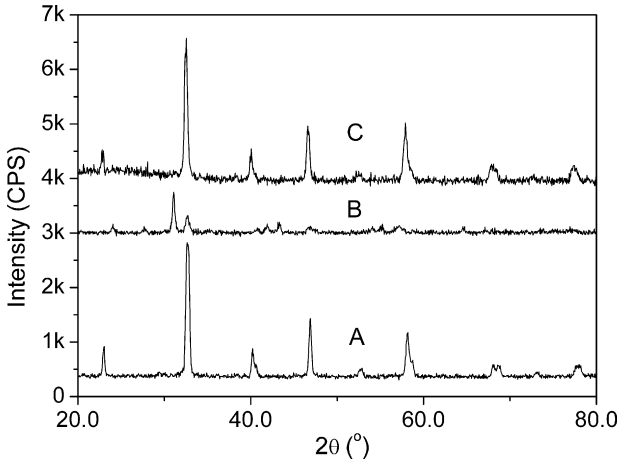

Fig. 11. XRD patterns of LSM material (A) LSM fresh; (B) LSM reduced by hydrogen at 600 °C and (C) the reduced LSM powder was treated with methane and air mixed gas for about 90 min at 800 °C.

I–P curves of the cell with an LSSM cathode at 750–850 °C. Before each test, the whole cell was treated under a hydrogen atmosphere for 1 h at 600 °C to reduce the NiO in the anode to Ni. Once the reduction was completed, the chamber atmosphere was switched to a methane–air mixed gas. As can be seen in Fig. 8, the steady state PPDs reached 240 and 202 mW cm^{-2} at 850 and 825 °C, respectively, which are comparable values to that of the cell initialized by ex situ reduction. This indicates that the in situ reduction process did not have an obvious effect on the structure and composition of the LSSM cathode. Such a conclusion is supported by the XRD results as shown in Fig. 9. It can be seen that the LSSM had stable perovskite structure after the pretreatment in a hydrogen atmosphere at 600 °C for an hour.

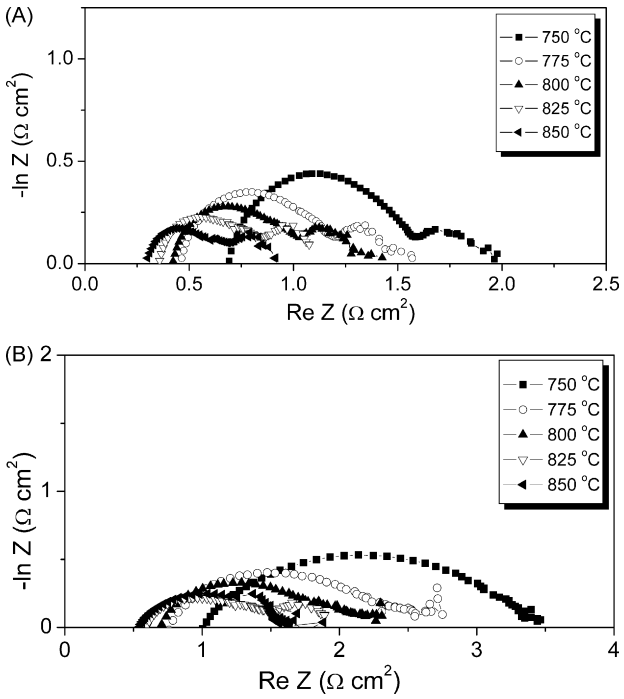

Fig. 13. The impedance of the cell with LSM cathode from the ex situ (A) and in situ (B) reduction method.

In order to further demonstrate the stability of LSSM in the process of the in situ reduction method, the performance of the cell with the LSM cathode was tested in the same way. As shown in Fig. 10, although this cell also showed a relatively stable performance after exposure to a methane and air mixture gas, it delivered a peak power density of just 90 mW cm^{-2} at 800 °C as compared to ~225 mW cm^{-2} for the cell following ex situ reduction. Based on the preliminary analysis of Fig. 11, the perovskite structure of the LSM was destroyed after the treatment in a hydrogen atmosphere at 600 °C for 1 h. This suggests that the phase reduction could be a cause for the reduced cell performance. However, it was reported that some perovskite materials have very good phase reversibility [16,20]; once the oxidant atmosphere was recovered, the reduced material could restore its perovskite phase structure at high temperature easily. Previously, we have demonstrated that the reduced BSCF could partially restore its perovskite structure after switching on a methane–air mixture at high temperature [20]. The phase reversibility of LSM was then tested. After the reduction of LSM by hydrogen, a mixed gas composed of methane and air with similar ratio for the single-chamber operation was switched on and treated

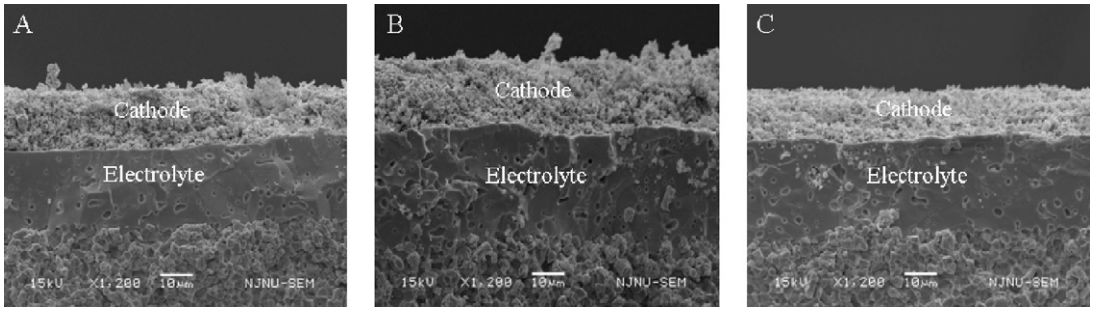

Fig. 12. (A)–(C) Cross-sectional SEM micrographs of the cell with LSM cathode (A) before reducing by hydrogen; (B) after reducing by hydrogen; (C) after re-oxidizing by methane and air mixed gases which were pre-treated with hydrogen.

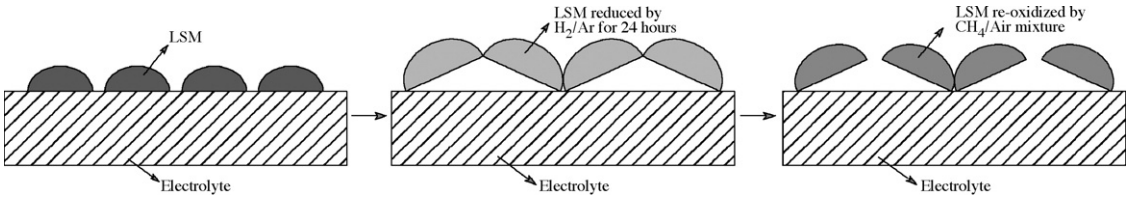

Fig. 14. The mechanism for the reduced cell performance via the in situ reduction for cell initialization.

at 800 °C for 1.5 h. As shown in Fig. 11C, the perovskite structure was perfectly restored. This suggests that the destruction of the phase structure by hydrogen may not be the reason for the reduced performance in the in situ reduction process for the cell initialization with the LSM cathode.

It is well known that the electrode performance is related with not only to the material's intrinsic properties, but also its microstructure. Fig. 12 shows the cross-sectional SEM photos of the cells with fresh, hydrogen-reduced and re-oxidized LSM cathode by methane and air mixed gas, respectively. There is no evidence clearing showing that the electrode microstructure changed significantly. However, Fig. 12 does not have the resolution to elucidate if there was structure change at the nano scale. The possible microstructure change in the microdomain of the LSM cathode during the reduction/re-oxidation process was supported by the impedances of the electrode. Fig. 13 shows the impedance spectroscopes of the cell with LSM initialized by in situ reduction and ex situ reduction, where it is clearly shown that the electrode polarization resistance and the ohmic resistance of the cell initialized by in situ reduction method are both larger than the cell initialized by the ex situ reduction method. To understand such a difference, the expansion properties of LSM and LSSM samples were applied. The samples were first pressed into quadrate bars, and then fired at 1400 °C for 5 h in air to get dense bars with an original size of 2.74 mm × 17.47 mm × 5.40 mm. After exposure to a 5% H_2/Ar atmosphere for 24 h at 900 °C, the volume of the LSM bar was found to increase by 5.0% of its original size, compared to 0.91% for the LSSM. Furthermore, it was also found that the crystallite sizes of fresh LSM and re-oxidized LSM were, 17.05 and 20.46 nm, respectively, i.e., the crystallite size was increased after the reduction/re-oxidation process. Based on the above analysis, a mechanism was proposed for the reduced cell performance via the in situ reduction for cell initialization, as shown in Fig. 14. During the in situ reduction process, the LSM was reduced, which led to the expansion of the oxide and caused a strong tension inside the electrode. To release the tension, some electrode–electrolyte connections were broken, which could happen on the nano scale. This then led to an increase in interfacial polarization resistance. During the oxidation process, the oxide shrank, which again created internal stress, such that some of the closely contacted electrode particles might separated during this oxidation process and resulting in an increase in contact resistance. Both points result in the deterioration of fuel cell performance by increasing the electrode polarization resistance and the ohmic resistance, as shown in Fig. 13.

4. Conclusions

$La_{0.8}Sr_{0.2}MnO_3$ and $La_{0.8}Sr_{0.2}Sc_{0.1}Mn_{0.9}O_3$ were synthesized and characterized as cathode materials of SC-SOFCs. LSSM had higher activity than LSM for the oxidization of methane because more oxygen vacancies were created due to the Sc^{3+} doping. Such oxygen vacancies also had a crucial role in oxygen reduction and methane oxidation. CH_4 and O_2 adsorbed on different active sites over both the LSM and LSSM cathodes. The cell with the LSSM cathode had lower OCVs than the cell with the LSM cathode due to the higher catalytic activity of LSSM for methane oxidation. The higher activity of LSSM for oxygen reduction along with its higher activity for methane oxidation than the LSM resulted in comparable power output for the cell with the LSSM cathode and the cell with the LSM cathode. The oxidation CO_2 product had a negligible effect on the oxygen reduction over both the LSM and LSSM cathode, which is a significant advantage for single-chamber fuel cell application. LSSM is amenable to in situ reduction due to its improved chemical stability. Similar performance was observed for the cells with LSSM cathode initialized by in situ reduction and ex situ reduction. However, LSM can be reduced under a hydrogen atmosphere. Although the phase reversibility of LSM is really good, the electrode morphology might be changed at the nano scale during the reduction and re-oxidation process, resulting in the reduced cathode performance. As a whole, LSSM is a promising SC-SOFC cathode material.

Acknowledgements

This work was supported by the National Natural Science Foundation of China under contract Nos. 20646002, 20676061 and 20703024, by the National 863 program under contract No. 2007AA05Z133, and by the National Basic Research Program of China under contract No. 2007CB209704.

References

[1] T. Hibino, A. Hashimoto, T. Inoue, J. Tokuno, S. Yoshida, M. Sano, Science 288 (2000) 2031–2033.
[2] Z.P. Shao, C. Kwak, S.M. Haile, Solid State Ionics 175 (2004) 39–46.
[3] T.W. Napporn, X. Jacques-Bedard, F. Morin, M. Meunier, J. Electrochem. Soc. 151 (2004) A2088–A2094.
[4] B.E. Buergler, M.E. Siegrist, L.J. Gauckler, Solid State Ionics 176 (2005) 1717–1722.
[5] T. Suzuki, P. Jasinski, V. Petrovsky, H.U. Anderson, F. Dogan, J. Electrochem. Soc. 152 (2005) A527–A531.
[6] I. Riess, P.J. van der Put, J. Schoonman, Solid State Ionics 82 (1995) 1–4.
[7] A.K. Demin, F.Y. Gulbis, Solid State Ionics 135 (2000) 451–456.
[8] T. Hibino, S.Q. Wang, S. Kakimoto, M. Sano, Solid State Ionics 127 (2000) 89–98.
[9] M.L. Liu, Z. Lü, B. Wei, R.B. Zhu, X.Q. Huang, K.F. Chen, G. Ai, W.H. Su, J. Electrochem. Soc. 154 (2007) B588–B592.
[10] Y. Hao, D.G. Goodwin, J. Power Sources 183 (2008) 157–163.
[11] X.G. Zhang, M. Robertson, S. Yick, C. Deces-Petit, E. Styles, W. Qu, Y.S. Xie, R. Hui, J. Roller, O. Kesler, R. Maric, D. Ghosh, J. Power Sources 160 (2006) 1211–1216.
[12] K.B. Yoo, G.M. Choi, J. Eur. Ceram. Soc. 27 (2007) 4211–4214.
[13] Y.B. Lin, S.A. Barnett, Solid State Ionics 179 (2008) 420–427.
[14] W. Zhou, Z.P. Shao, R. Ran, P.Y. Zeng, H.X. Gu, W.Q. Jin, N.P. Xu, J. Power Sources 168 (2007) 330–337.
[15] Y. Lin, R. Ran, Y. Zheng, Z.P. Shao, W.Q. Jin, N.P. Xu, J. Ahn, J. Power Sources 180 (2008) 15–22.
[16] Z.P. Shao, W.S. Yang, Y. Cong, H. Dong, J.H. Tong, G.X. Xiong, J. Membr. Sci. 172 (2000) 177–188.
[17] Z.P. Shao, S.M. Haile, Nature 431 (2004) 170–173.
[18] Z.P. Shao, S.M. Haile, J. Ahn, P.D. Ronney, Z.L. Zhan, S.A. Barnett, Nature 435 (2005) 795–798.
[19] Y. Hao, Z. Shao, J. Mederos, W. Lai, D.G. Goodwin, S.M. Haile, Solid State Ionics 177 (2006) 2013–2021.
[20] C.M. Zhang, Y. Zheng, R. Ran, Z.P. Shao, W.Q. Jin, N.P. Xu, J. Ahn, J. Power Sources 179 (2008) 640–648.
[21] S.P. Jiang, J.G. Love, Solid State Ionics 138 (2001) 183–190.
[22] H.X. Gu, Y. Zheng, R. Ran, Z.P. Shao, W.Q. Jin, N.P. Xu, J. Ahn, J. Power Sources 183 (2008) 471–478.
[23] Y. Zheng, R. Ran, H.X. Gu, R. Cai, Z.P. Shao, J. Power Sources 185 (2008) 641–648.
[24] Y. Zheng, C.M. Zhang, R. Ran, R. Cai, Z.P. Shao, D. Farrusseng, Acta Mater. 57 (2008) 1165–1175.
[25] Y. Zheng, R. Ran, Z.P. Shao, J. Phys. Chem. C 112 (2008) 18690–18700.

[26] X.L. Yue, A.Y. Yan, M. Zhang, L. Liu, Y.L. Dong, M.J. Cheng, J. Power Sources 185 (2008) 691–697.
[27] W. Zhou, Z.P. Shao, W.Q. Jin, J. Alloys Compd. 426 (2006) 368–374.
[28] H.X. Gu, R. Ran, W. Zhou, Z.P. Shao, J. Power Sources 172 (2007) 704–712.
[29] M. Kilo, J. Weigel, A. Wokaun, R.A. Koeppel, A. Stoeckli, A. Baiker, J. Mol. Catal. A: Chem. 126 (1997) 169–184.
[30] L. Ge, W. Zhou, R. Ran, Z.P. Shao, S.M. Liu, J. Alloys Compd. 450 (2008) 338–347.
[31] S.B. Adler, Chem. Rev. 104 (2004) 4791–4843.
[32] R.J. Bell, G.J. Millar, J. Drennan, Solid State Ionics 131 (2000) 211–220.
[33] P.D. Petrolekas, I.S. Metcalfe, J. Catal. 152 (1995) 147–163.
[34] A.Y. Yan, M.J. Cheng, W.S. Yang, V. Maragou, S.Q. Song, P. Tsiakaras, Appl. Catal. B: Environ. 66 (2006) 64–71.
[35] A.Y. Yan, M. Yang, Z.F. Hou, Y.L. Dong, M.J. Cheng, J. Power Sources 185 (2008) 76–84.
[36] P. Decorse, G. Caboche, L. Dufour, Solid State Ionics 117 (1999) 161–169.
[37] M.M. Viitanen, R.G. van Welzenis, H.H. Brongersma, F.P.F. van Berkel, Solid State Ionics 150 (2002) 223–228.
[38] Y. Jiang, S.Z. Wang, Y.H. Zhang, J.W. Yan, W.Z. Li, J. Electrochem. Soc. 145 (1998) 373–378.
[39] H.Y. Lee, W.S. Cho, S.M. Oh, H.D. Wiemh fer, G.W. pel, J. Electrochem. Soc. 142 (1995) 2659–2664.
[40] W. Wang, S.P. Jiang, Solid State Ionics 177 (2006) 1361–1369.